Letter

Superconductivity and fermionic dissipation in quantum Hall edges

Noam Schiller,[1,*] Barak A. Katzir,[2,*] Ady Stern,[1] Erez Berg,[1] Netanel H. Lindner,[2] and Yuval Oreg[1]
[1]*Department of Condensed Matter Physics, Weizmann Institute of Science, Rehovot 76100, Israel*
[2]*Physics Department, Technion, Haifa 320003, Israel*

(Received 21 March 2022; accepted 20 March 2023; published 11 April 2023)

Proximity-induced superconductivity in fractional quantum Hall edges is a prerequisite to proposed realizations of parafermion zero modes. A recent experimental work [Gül *et al.*, Phys. Rev. X **12**, 021057 (2022)] provided evidence for such coupling, in the form of a crossed Andreev reflection signal, in which electrons enter a superconductor from one chiral mode and are reflected as holes to another, counterpropagating chiral mode. Remarkably, while the probability for crossed Andreev reflection was small, it was stronger for $\nu = 1/3$ fractional quantum Hall edges than for integer ones. We theoretically explain these findings, including the relative strengths of the signals in the two cases and their qualitatively different temperature dependencies. An essential part of our model is the coupling of the edge modes to normal states in the cores of Abrikosov vortices induced by the magnetic field, which provide a fermionic bath. We find that the stronger crossed Andreev reflection in the fractional case originates from the suppression of electronic tunneling between the fermionic bath and the fractional quantum Hall edges. Our theory shows that the mere observation of crossed Andreev reflection signal does not necessarily imply the presence of localized parafermion zero modes, and suggests ways to identify their presence from the behavior of this signal in the low-temperature regime.

DOI: 10.1103/PhysRevB.107.L161105

Introduction. Topological quantum computation (TQC) benefits from resilience to errors arising from local noise and decoherence processes [1,2]. In particular, such protection is obtained by encoding the quantum data in many-body systems which harbor a non-Abelian phase of matter. These phases are characterized by having an energy gap and nontrivial ground state degeneracy in the presence of specific quasiparticles or defects [3].

The most well-studied non-Abelian phases are those supporting Majorana zero modes (MZMs). Notable examples of systems realizing such phases are the Moore-Read fractional quantum Hall state [4,5], $p + ip$ superconductors [6,7], and arrays of p-wave superconducting wires [8–11]. While currently being the most experimentally accessible non-Abelian systems, MZMs do not admit universal TQC [12]. Beyond the MZM paradigm, phases admitting parafermion zero modes (PZMs) support a richer set (yet not universal) of topologically protected quantum gates induced by braiding [12]. Furthermore, systems supporting universal TQC can be realized by utilizing an array of PZMs [13].

A promising method to realize PZMs utilizes proximity coupling between a superconductor (SC) and counterpropagating fractional quantum Hall (FQH) edge modes [14–18] (other routes towards realizing PZMs [19–23] and various experimental signatures [24–28] have been proposed as well). Importantly, to sustain PZMs suitable for TQC, this coupling must induce an energy gap. This requires overcoming two major obstacles. First, the gap can be impeded by repulsive electron-electron interactions within the edges. This obstacle can be overcome for judicious choices of physical parameters [29]. The second challenge, and the focus of this Letter, is that the high magnetic fields required to sustain the FQH state clash with superconductivity. This leads to a proliferation of in-gap states, such as those residing in the cores of Abrikosov vortices in the superconductor supplying the proximity coupling [30–32]. By electron tunneling between these states and the edge modes, current can be conveyed out of the system through a grounded reservoir connected to the superconductor, serving as a source of fermionic dissipation.

Despite these challenges, systems of SCs proximity coupled to QH edge modes have been subject to much interest. This includes theoretical approaches to predict transport measurements of these systems [33–36], and experimental works showing promising results in graphene [37–41]. In particular, Ref. [37] successfully confirmed proximity coupling of both integer quantum Hall (IQH) and FQH states via the observation of crossed Andreev reflection (CAR) across the superconductor. Notably [see Fig. 5(f) in Ref. [37]], the probability of CAR was larger for Laughlin FQH states than IQH; however, in both cases, this probability was significantly smaller than 1, hinting that fermionic dissipation plays a major role. In the IQH case, the CAR probability was largely temperature independent. In contrast, the proximitized Laughlin FQH edges displayed a CAR signal that grows with decreasing temperature, raising the hope that the system approaches the local PZM-harboring phase in the zero-temperature limit.

Motivated by these results, in this Letter we introduce a model to treat the effects of vortices on electric transport QH-SC hybrid systems. Our model includes three types of processes: dissipation via single-electron tunneling into vortex core states; backscattering between edges; and crossed

[*]These authors contributed equally to this work.

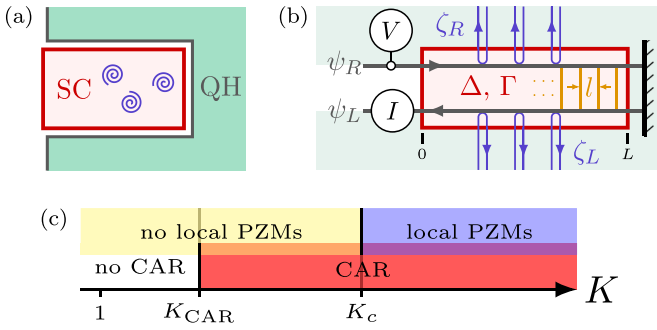

FIG. 1. (a) The physical system: a quantum Hall (QH) droplet, with its edge proximity coupled to a superconductor (SC) in a "finger" shape. Due to the strong magnetic field, Abrikosov vortices are present in the SC finger and act, due to their normal core, as a metallic bath. (b) The model, Eq. (1): The boundary of a QH droplet at filling factor $\nu = 1/m$ (for odd integer m) is modeled by two edge modes, $\psi_{R/L}(x)$, counterpropagating along a grounded SC finger of length L. The right-moving mode arrives at the finger region $x = 0$ at bias V, and is totally backscattered at $x = L$ into a left-moving edge mode that leaves the finger region at $x = 0$. The counterpropagating edges are proximity coupled to the SC finger, and are subject to backscattering and Andreev reflection between the edges. We denote the tunneling amplitudes of these two processes by Γ and Δ, respectively. The dissipative vortices are modeled as one-dimensional metallic modes $\zeta_{R/L}$ coupled at each point along the finger to the QH edges. (c) A phase diagram of a fractional model with $m > 2$ as a function of the Luttinger parameter K. Above $K > K_{\mathrm{CAR}}$ there is the onset of CAR correlations. At $K = K_c$ we find a phase transition to a local PZM-harboring phase.

Andreev reflection via the superconductor. We note that while dissipation has been studied in Luttinger liquids in various contexts [42–45], this is typically done via density-density interactions with some external environment, rather than fermionic dissipation in which electrons directly tunnel into a metallic environment.

Calculating the electric conductance in the dissipation-dominated regime, we find qualitatively different behavior for IQH-SC and Laughlin FQH-SC hybrid systems. For the IQH states, the conductance saturates at low energies to a negative value if interedge Andreev reflection is stronger than interedge backscattering, and to a positive value otherwise. Conversely, FQH states may display an enhancement of CAR with lowering temperatures over a wide temperature range, bounded from below by a temperature determined by the size of the system. This occurs if the effective interactions on the FQH edge are sufficiently attractive, as a result of the presence of the superconductor. Interestingly, while in the IQH case dissipation always spoils the robustness of localized zero modes, the FQH case exhibits two phases in which a CAR signal persists, one of which supports localized PZMs [see Fig. 1(c)]. The distinction between the integer and fractional cases results from the suppression of fractional quasiparticle tunneling into the vortex core states [46–49]. Our results are congruent with the aforementioned reporting of larger CAR for fractional versus integer states in Ref. [37].

Model. We model the system as described in Fig. 1(b). A superconductor of length L is embedded within the bulk of a Laughlin FQH state at filling factor $\nu = 1/m$ for odd integer m. We describe the QH edge in terms of two modes, converging at the end of the finger: a right-moving mode, which emanates towards the finger from a reservoir at bias voltage V, and a left-moving mode, which is collected by a grounded reservoir. We denote the current collected at this reservoir as I.

Within the superconductor, we model the presence of vortices as a continuum of metallic states, justified by the dense spacing of the vortex core Caroli–de Gennes–Matricon states [32]. We thus treat these states as metallic quasi-one-dimensional leads, with an effective "Fermi velocity" corresponding to the normal NbN density of states. We assume that vortices are sufficiently prevalent such that these states are available throughout the edge. Three processes are enabled within the finger: backscattering between the edges; crossed Andreev reflection (CAR) via the superconductor; and tunneling into the metallic states. These processes are characterized phenomenologically by tunneling amplitudes of Γ, Δ, and w, respectively.

We define right- and left-moving boson fields, with the electron's annihilation operators being $\psi_{R/L} = e^{\pm im\phi_{R/L}}/\sqrt{2\pi a}$, where a is a short-distance cutoff of the order of the magnetic length [50]. The boson operator fields satisfy the commutation relations $[\phi_{R/L}(x), \phi_{R/L}(y)] = \pm i\pi\,\mathrm{sgn}(x-y)/m$ and $[\phi_L(x), \phi_R(y)] = i\pi/m$. The corresponding electric charge and current densities are $\hat{\rho}_{R/L} = \partial_x\phi_{R/L}/(2\pi)$ and $\hat{j}_{R/L} = -\partial_t\phi_{R/L}/(2\pi)$, respectively.

The Hamiltonian of the system is given in terms of the bosonized fields by $\mathcal{H} = H_0 + H_\zeta + H_\Gamma + H_\Delta + H_w$ [50,51], where

$$
\begin{aligned}
H_0 &= \frac{m}{4\pi}\int_{-\infty}^{L} dx\{v[(\partial_x\phi_R)^2+(\partial_x\phi_L)^2]+2U(\partial_x\phi_R)(\partial_x\phi_L)\},\\
H_\zeta &= \sum_{\gamma=R,L}\int dx\,dy\,\zeta_\gamma^\dagger(x,y)(-iv_b\partial_y)\zeta_\gamma(x,y),\\
H_\Gamma &= \frac{\Gamma}{\pi a^2}\int_0^L dx\cos(m\phi_R + m\phi_L),\\
H_\Delta &= \frac{\Delta}{\pi a^2}\int_0^L dx\cos(m\phi_R - m\phi_L),\\
H_w &= \sum_{\gamma=R,L}\int_0^L dx\left[\frac{w}{\sqrt{a}}\,\psi_\gamma^\dagger(x)\zeta_\gamma(x,y=0)+\mathrm{H.c.}\right].
\end{aligned}
\tag{1}
$$

Here, v and v_b are Fermi velocities of the FQH edge and the metallic states, respectively, U is the interaction strength between the two edges, $\zeta_{R/L}$ annihilates an electron in a metallic mode that couples to the right/left-moving edge, and we chose the units such that $\hbar = 1$. These define the Luttinger velocity $u = \sqrt{v^2 - U^2}$ and the Luttinger parameter $K = \sqrt{\frac{v-U}{v+U}}$. Notice that Γ, Δ, w, and U all carry units of velocity. We assume that the edges are spin polarized and the superconductor has sufficient spin-orbit coupling to induce pairing between them.

We proceed by integrating out the bath degrees of freedom. A calculation of the perturbative renormalization group (RG) flow equations with respect to the Luttinger liquid fixed point H_0 is straightforward and yields (see Sec. B of the Supple-

mental Material [52])

$$\frac{d\Delta}{d\ell} = (2 - m/K)\Delta, \quad \frac{d\Gamma}{d\ell} = (2 - mK)\Gamma,$$
$$\frac{d\alpha}{d\ell} = (2 - m\bar{K})\alpha, \quad \frac{du}{d\ell} = -2m\bar{K}\alpha, \tag{2}$$
$$\frac{dK}{d\ell} = m\left(\frac{\Delta}{u}\right)^2 - mK^2\left(\frac{\Gamma}{u}\right)^2 + m\frac{\alpha}{u}(1 - K^2),$$

where $\alpha = |w|^2/(2\pi v_b)$, and $\bar{K} = (K + K^{-1})/2$.

We see that all three processes are relevant for IQH edges, and irrelevant for noninteracting FQH edges. In FQH edges, Andreev reflection becomes relevant for sufficiently attractive interactions, $K > K_c = m/2$; importantly, Andreev reflection becomes the least irrelevant process at weaker attractive interactions, $K > K_{\mathrm{CAR}} = \frac{\sqrt{3m^2+4}-2}{m}$. The phase boundaries are obtained by examining the equation for K and comparing the scaling of Δ^2, Γ^2, and α which appear in this equation. In the FQH case this admits a regime, $K_{\mathrm{CAR}} < K < K_c$, that does not support localized PZMs, but can exhibit CAR at nonzero temperatures. A schematic phase diagram is shown in Fig. 1(c).

Temperature-dependent perturbative solution. We calculate transport properties of the system perturbatively in all three couplings. The RG equation for K shows that, for IQH in the dissipation-dominated regime, the system flows towards $K = 1$. As such, in the IQH case, we set $K = 1$.

For the perturbative calculation, we imagine dividing the finger into multiple segments of equal length l, such that each segment is close to local equilibrium. This enables us to define a local voltage for each segment, $V_{R/L}(x_n)$, $x_n = nl$. Furthermore, we assume that propagating quasiparticles lose coherence between segments, formally implemented by neglecting intersegment correlations. In essence, we treat each segment as a quantum resistor, and the resulting network of resistors is treated classically. Motivated by the strong dissipation apparent in the experimental data, we assume that we are in the dissipation-dominated regime. In this regime, we take the segment length scale l to be the dissipation length l_d, defined as the length scale at which most of the current dissipates into the vortices.

We proceed by writing continuity equations for the right- and left-moving densities, $\partial_t \hat{\rho}_{R/L} = -i[\hat{\rho}_{R/L}, \mathcal{H}]$. Taking expectation values with respect to the unperturbed Hamiltonian H_0, and restricting ourselves to steady states $\langle \partial_t \hat{\rho}_{R/L} \rangle = 0$, we find a "Kirchhoff-like" equation relating the currents at boundaries between segments, given at the small segment limit $l_d \ll L$ by

$$\langle \partial_x \hat{j}_R(x) \rangle = -\langle \hat{J}_\Gamma(x) \rangle - \langle \hat{J}_\Delta(x) \rangle - \langle \hat{J}_{w,R}(x) \rangle,$$
$$\langle \partial_x \hat{j}_L(x) \rangle = -\langle \hat{J}_\Gamma(x) \rangle + \langle \hat{J}_\Delta(x) \rangle + \langle \hat{J}_{w,L}(x) \rangle. \tag{3}$$

Here, the operators on the right-hand side (RHS) denote the three processes that current can undergo in each segment: $\hat{J}_\Gamma$ describes the current per unit length that backscatters from the right-moving to the left-moving edge; $\hat{J}_\Delta$ describes the Andreev current per unit length which flows from the edges into the superconductor; and $\hat{J}_{w,R/L}$ describes the current per unit length that dissipates from the right/left-moving edge to the metallic states.

The expectation values of all the operators are evaluated perturbatively to leading orders in $|\Delta|^2$, $|\Gamma|^2$, and α. Within this treatment, the left-hand side (LHS) of Eq. (3) is given by $\langle \hat{j}_{R/L}(x_i) \rangle = \sigma_{xy} V_{R/L}(x_i)$, where σ_{xy} is the Hall conductance. The RHS is calculated in Sec. C of the Supplemental Material [52]. Due to the lack of coherence between segments, the expectation values depend on the voltage in a local manner.

At nonzero temperature and sufficiently low voltages, $eV \ll k_B T$, each quantum resistor is at the Ohmic limit. Explicit calculation then gives, for each segment, $\langle \hat{J}_\Gamma(x) \rangle = \frac{e^2}{u^2 a} A_\Gamma |\Gamma|^2 [V_R(x) - V_L(x)]$, $\langle \hat{J}_\Delta(x) \rangle = \frac{e^2}{u^2 a} A_\Delta |\Delta|^2 [V_R(x) + V_L(x)]$, and $\langle \hat{J}_{w,R/L}(x) \rangle = \frac{e^2}{ua} A_w \alpha V_{R/L}(x)$, where $A_c(T)$ with $c = \Gamma, \Delta, w$ are unitless coefficients that encode temperature dependence, and we suppress the T dependence for brevity. The derivation and explicit forms of the $A_c(T)$ coefficients are given in Sec. C of the Supplemental Material [52] (see Table C1). We plug these values into Eq. (3), and solve it with the boundary conditions $V_R(0) = V$ (representing the incoming bias voltage) and $V_R(L) = V_L(L)$ (representing the edge of the finger, where all remaining right movers become left movers). The collected current is given by $I = \sigma_{xy} V_L(0)$.

The full solution for a general L is given in Eq. (C20) in the Supplemental Material [52]. At the infinite finger limit, $L \to \infty$, we obtain the result

$$\frac{V_L(0)}{V} = \frac{A_\Gamma |\Gamma|^2 - A_\Delta |\Delta|^2}{A_\Gamma |\Gamma|^2 + A_\Delta |\Delta|^2 + u A_w \alpha + \lambda}, \tag{4}$$

where for convenience we define $(\lambda \frac{e}{hm})^2 \equiv (A_\Gamma |\Gamma|^2 + A_\Delta |\Delta|^2 + u A_w \alpha)^2 - (A_\Gamma |\Gamma|^2 - A_\Delta |\Delta|^2)^2$. As such, even in the case where all three processes are irrelevant, the low-energy behavior is dominated by the process which is *least* irrelevant, with differential conductance at zero temperature taking a well-quantized value of $G/\sigma_{xy} = \pm 1, 0$. Andreev reflection becomes the least irrelevant process at $K > K_{\mathrm{CAR}}$, whereas it becomes relevant at $K > K_c$; in particular, for $m = 3$ a low-energy CAR signature is obtained without localized PZMs in the range $1.19 \lesssim K < 1.5$. Notice that a crossover between negative and positive conductance can occur if $(A_\Gamma |\Gamma|^2 - A_\Delta |\Delta|^2)$ changes sign at a nonzero temperature (see Fig. 2).

Microscopic details, such as the coherence length (∼50 nm for NbN) and penetration depth (200–300 nm) of the superconductor, and the metallic density of states (which is related to the Δ^2/E_F level spacing of the Caroli–de Gennes–Matricon states [32]), enter the model through the three bare tunneling amplitudes. As such, variance in these parameters will not affect the RG flow of Eq. (2), nor will they effect the qualitative phase boundaries in Fig. 1(c). Such variance will, however, affect the precise measured conductance of Fig. 2 (compare solid to dashed lines).

Finite L affects the behavior at very low temperatures. At finite L and $m > 1$, the temperature dependence of l_d defines a temperature scale at which $l_d(T_{\mathrm{fs}}) \sim L$. It is reasonable to surmise that at $T \ll T_{\mathrm{fs}}$ all three processes flow to zero, such that all current flows back and forth around the entire finger unperturbed, yielding $G \to \sigma_{xy}$.

In Figs. 2 and 3, we plot the temperature dependence of the differential conductance, $G \equiv dI/dV$ for noninteracting IQH

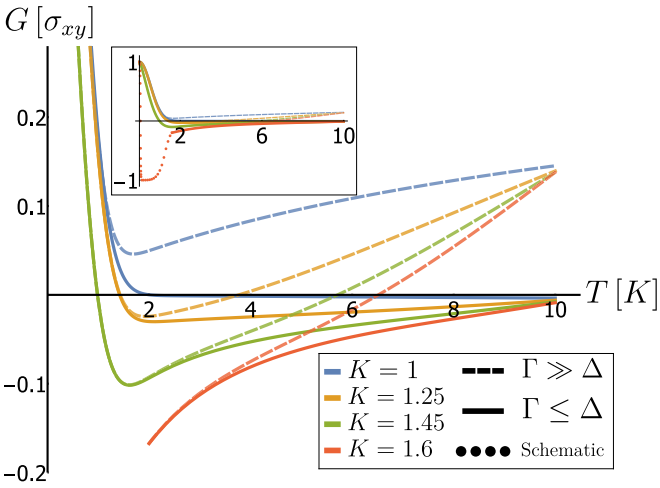

FIG. 2. Differential conductance $G \equiv dI/dV$ (normalized by Hall conductance) as a function of temperature for Laughlin fractional edges ($m = 3$) and various Luttinger parameters K, as obtained from a solution of Eq. (3). The results displayed are for a system length of $L = 2$ μm, a backscattering length of $(|\Gamma|^2/4\pi u^2 a)^{-1} = 100$ nm (dashed lines) or $(|\Gamma|^2/4\pi u^2 a)^{-1} = 2$ μm (solid lines), an Andreev-reflection length of $(|\Delta|^2/4\pi u^2 a)^{-1} = 1.6$ μm, a dissipation length of $(|w|^2/u v_b a)^{-1} = 10$ nm, a Luttinger velocity of $u = 2.5 \times 10^4$ m/s, and a short-distance cutoff of $a = 7$ nm, such that we are in the regime where bare dissipation dominates bare backscattering and Andreev reflection. We see that, over a range of low temperatures comparable to experimental data in Ref. [37], CAR increases with decreasing temperature for sufficiently attractive interactions ($K > K_{\mathrm{CAR}}$). Inset: At sufficiently low temperatures, the finite size of the finger causes conductance to rise back to σ_{xy}. As a function of system size, this transition temperature decays as a power law for $K < K_c = 1.5$, and exponentially for $K > K_c$ (schematically drawn with the dotted line). Just above this transition temperature, the $K > K_c$ case is near the full Andreev reflection fixed point, driving the conductance to $-\sigma_{xy}$.

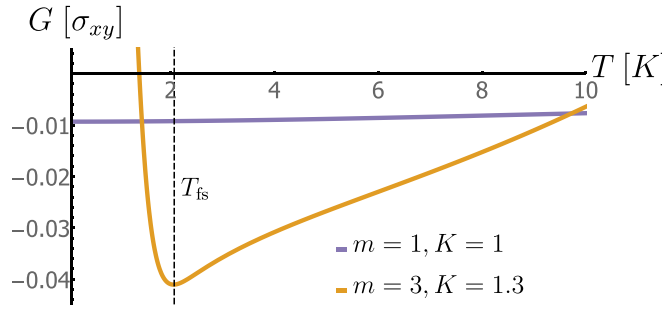

FIG. 3. Differential conductance $G \equiv dI/dV$ (normalized by Hall conductance) as a function of temperature for noninteracting integer edges ($m = 1$, $K = 1$) (purple curve) and attractively interacting Laughlin fractional edges ($m = 3$, $K = 1.3$) (orange curve), as obtained from a solution of Eq. (3). We choose the same parameters as the solid lines in Fig. 2, such that we are in the regime where bare dissipation dominates bare backscattering and Andreev reflection. At the low-temperature limit we show here that CAR saturates for electrons, having a very weak dependence on the temperature. For fractional quasiparticles, CAR grows monotonously with decreasing temperature over a wide range, bounded from below by T_{fs} (dashed vertical line), at which point the finite size of the finger causes conductance to collapse to σ_{xy}. From the RG equations (2) we see that the velocity u decreases at low energies, an effect we neglected in Eq. (4); as such, the value of T_{fs} shown here is an overestimate.

$(m = 1, K = 1)$ and for $\nu = 1/3$ FQH edges, respectively. We choose parameters that enable significant CAR, and give a high-energy cutoff of ∼10 K, consistent, for example, with a bulk gap of 20 K found experimentally [53]. Indeed, for noninteracting IQH edges, CAR plateaus at low temperatures. For $\nu = 1/3$ edges, conversely, CAR increases as temperature decreases when interactions are sufficiently attractive, $K > K_{\mathrm{CAR}}$. This process continues until the finite size of the finger demands that all irrelevant processes halt and all current is reflected from the end of the finger.

For even stronger interactions ($K > K_c$), the Andreev pairing is relevant, and the system is driven towards a local PZM-harboring phase. At this point, Eq. (4) is no longer valid. For comparison, the red dotted curve in the inset of Fig. 2 shows a schematic temperature dependence of a power-law decay to the Andreev reflection fixed point [24], with a finite-size effect at low enough temperatures.

Overall, our model reproduces the temperature-dependent features seen in Ref. [37] [in particular Fig. 5(f)], without requiring the proximity to the superconductor to drive the system to a local PZM-harboring phase.

Exact solution for the $\nu = 1$ case. We also ascertain the validity of our model by analyzing the case of IQH, in which our model can be written as a noninteracting electron system. The Hamiltonian in Eq. (1) is quadratic in fermionic operators and is exactly solvable. We obtain a nonperturbative expression for the scattering matrix and the differential conductance, with the derivation given in Sec. A of the Supplemental Material [52]. We then continue to compare the temperature dependence of the conductance as calculated in the exact solution and the perturbative analysis discussed above. Moreover, we compare the conductance dependence on bias between the exact solution and the experimental data of [37]. In the absence of dissipation and at the limit $L \to \infty$, we obtain the known result

$$dI/dV|_{V=0} = (e^2/h)\,\mathrm{sgn}\{|\Gamma| - |\Delta|\}. \tag{5}$$

These two possible values correspond to the two symmetry protected phases of Kitaev's wire model [8]. In the presence of dissipation we expect $|dI/dV| < e^2/h$.

For finite finger length L we find Tomasch oscillations [54], i.e., an interference effect due to reflection from both ends of the finger, with an associated energy period $E_{\mathrm{osc.}} = hu/(2L)$. Note that these interference effects are not incorporated in the previous perturbative calculations of Eqs. (4). Note that the experimental data in Ref. [37] show an asymmetric bias dependence. To explain this feature, we use a complex valued $\Gamma = |\Gamma|e^{i\theta}$ which breaks bias symmetry for electrons. This allows us to qualitatively fit the experimental data of Ref. [37] using our model parameters, as shown in Fig. 4.

Other FQH states. So far, we compared the $\nu = 1$ IQH state and the $\nu = 1/m$ Laughlin FQH states, which feature a single edge mode. States with multiple edge modes require more delicate treatment. Qualitatively, we expect the effect of vortices on such states to depend on the relevance

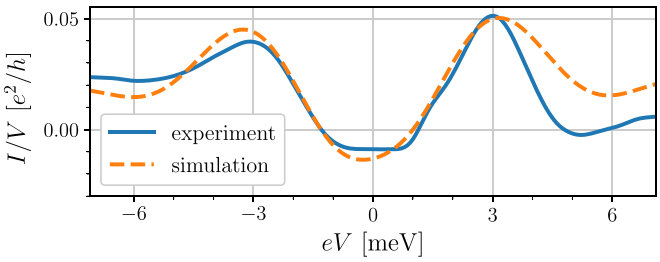

FIG. 4. Comparison between exact electron conductance I/V of model (1) in the noninteracting IQH case and the data of Ref. [37] [Fig. 11(f)]. The model parameters are $|\Delta/a| = 2.64$ meV, $|\Gamma/a| = 2.83$ meV, $2\pi\alpha/a = 2.8$ meV, $E_{\text{osc.}} = 4.06$ meV, and $\theta = 0.9\pi$.

of electron tunneling between the particular edge and the vortex core states. Interestingly, we find that (see Sec. D of the Supplemental Material [52]) for $\nu = 2/3$ this tunneling is marginal [55], while for $\nu = 2/5$ electron tunneling is irrelevant. This is consistent with the behavior seen in the experiment [37] [in particular Fig. 5(f)], in which the conductance at $\nu = 2/3$ plateaus at low temperature as in the $\nu = 1$ case, while the conductance for $\nu = 2/5$ is similar to that seen for $\nu = 1/3$.

In summary, the ultimate cause for the qualitatively different behavior we find in various quantum Hall states is the different level of suppression of electron tunneling into metallic reservoirs [46]. When this suppression is strong enough, it allows for a phase that supports local PZMs even in the presence of dissipation, and allows an enhanced CAR signal relative to that obtained in the IQH case.

Acknowledgments. We thank Eduardo Fradkin, Önder Gül, Ke Huang, Philip Kim, Omri Lesser, Yuval Ronen, and Jun Zhu for useful discussions, Evgenii Zheltonozhskii for useful comments on the original manuscript, and Önder Gül, Philip Kim, and Yuval Ronen for graciously sharing experimental data. This work was supported by the European Union's Horizon 2020 research and innovation programme (Grant Agreements LEGOTOP No. 788715, HQMAT No. 817799, and TOPFRONT No. 639172), the DFG (CRC/Transregio 183, EI 519/7-1), the BSF and NSF (2018643), and the ISF Quantum Science and Technology (2074/19). N.S. was supported by the Clore Scholars Programme.

[1] A. Kitaev, Ann. Phys. **303**, 2 (2003).
[2] C. Nayak, S. H. Simon, A. Stern, M. Freedman, and S. Das Sarma, Rev. Mod. Phys. **80**, 1083 (2008).
[3] A. Stern, Nature (London) **464**, 187 (2010).
[4] G. Moore and N. Read, Nucl. Phys. B **360**, 362 (1991).
[5] A. Stern, Ann. Phys. **323**, 204 (2008).
[6] N. Read and D. Green, Phys. Rev. B **61**, 10267 (2000).
[7] D. A. Ivanov, Phys. Rev. Lett. **86**, 268 (2001).
[8] A. Kitaev, Phys. Usp. **44**, 131 (2001).
[9] Y. Oreg, G. Refael, and F. von Oppen, Phys. Rev. Lett. **105**, 177002 (2010).
[10] R. M. Lutchyn, J. D. Sau, and S. Das Sarma, Phys. Rev. Lett. **105**, 077001 (2010).
[11] A. Cook and M. Franz, Phys. Rev. B **84**, 201105(R) (2011).
[12] The set of quantum gates associated with both TQC based on MZMs and PZMs is limited to qubit and qudit Clifford gates, respectively, and as such is nonuniversal.
[13] R. S. K. Mong, D. J. Clarke, J. Alicea, N. H. Lindner, P. Fendley, C. Nayak, Y. Oreg, A. Stern, E. Berg, K. Shtengel, and M. P. A. Fisher, Phys. Rev. X **4**, 011036 (2014).
[14] N. H. Lindner, E. Berg, G. Refael, and A. Stern, Phys. Rev. X **2**, 041002 (2012).
[15] D. J. Clarke, J. Alicea, and K. Shtengel, Nat. Commun. **4**, 1348 (2013).
[16] M. Cheng, Phys. Rev. B **86**, 195126 (2012).
[17] A. Vaezi, Phys. Rev. B **87**, 035132 (2013).
[18] J. Alicea and P. Fendley, Annu. Rev. Condens. Matter Phys. **7**, 119 (2016).
[19] F. Zhang and C. L. Kane, Phys. Rev. Lett. **113**, 036401 (2014).
[20] C. P. Orth, R. P. Tiwari, T. Meng, and T. L. Schmidt, Phys. Rev. B **91**, 081406(R) (2015).
[21] C. Fleckenstein, N. T. Ziani, and B. Trauzettel, Phys. Rev. Lett. **122**, 066801 (2019).
[22] M. Barkeshli, C.-M. Jian, and X.-L. Qi, Phys. Rev. B **87**, 045130 (2013).
[23] M. Barkeshli, Y. Oreg, and X.-L. Qi, arXiv:1401.3750.
[24] N. Schiller, E. Cornfeld, E. Berg, and Y. Oreg, Phys. Rev. Res. **2**, 023296 (2020).
[25] A. B. Michelsen, T. L. Schmidt, and E. G. Idrisov, Phys. Rev. B **102**, 125402 (2020).
[26] K. Snizhko, R. Egger, and Y. Gefen, Phys. Rev. B **97**, 081405(R) (2018).
[27] K. Snizhko, F. Buccheri, R. Egger, and Y. Gefen, Phys. Rev. B **97**, 235139 (2018).
[28] I. E. Nielsen, K. Flensberg, R. Egger, and M. Burrello, Phys. Rev. Lett. **129**, 037703 (2022).
[29] B. A. Katzir, A. Stern, E. Berg, and N. H. Lindner, arXiv:2011.13950.
[30] P. G. De Gennes and P. A. Pincus, *Superconductivity of Metals and Alloys* (CRC Press, Boca Raton, FL, 2019).
[31] M. Tinkham, *Introduction to Superconductivity*, Dover Books on Physics Series (Dover, New York, 2004).
[32] C. Caroli, P. G. De Gennes, and J. Matricon, Phys. Lett. **9**, 307 (1964).
[33] A. L. R. Manesco, I. M. Flór, C.-X. Liu, and A. R. Akhmerov, SciPost Phys. Core **5**, 045 (2022).
[34] A. B. Michelsen, P. Recher, B. Braunecker, and T. L. Schmidt, Phys. Rev. Res. **5**, 013066 (2023).
[35] T. H. Galambos, F. Ronetti, B. Hetényi, D. Loss, and J. Klinovaja, Phys. Rev. B **106**, 075410 (2022).
[36] V. D. Kurilovich, Z. M. Raines, and L. I. Glazman, arXiv:2201.00273.
[37] O. Gül, Y. Ronen, S. Y. Lee, H. Shapourian, J. Zauberman, Y. H. Lee, K. Watanabe, T. Taniguchi, A. Vishwanath, A. Yacoby, and P. Kim, Phys. Rev. X **12**, 021057 (2022).

[38] G.-H. Lee, K.-F. Huang, D. K. Efetov, D. S. Wei, S. Hart, T. Taniguchi, K. Watanabe, A. Yacoby, and P. Kim, Nat. Phys. **13**, 693 (2017).
[39] M. Hatefipour, J. J. Cuozzo, J. Kanter, W. Strickland, T.-M. Lu, E. Rossi, and J. Shabani, Nano Lett. **22**, 6173 (2022).
[40] F. Amet, C. T. Ke, I. V. Borzenets, J. Wang, K. Watanabe, T. Taniguchi, R. S. Deacon, M. Yamamoto, Y. Bomze, S. Tarucha, and G. Finkelstein, Science **352**, 966 (2016).
[41] L. Zhao, E. G. Arnault, A. Bondarev, A. Seredinski, T. Larson, A. W. Draelos, H. Li, K. Watanabe, T. Taniguchi, F. Amet, H. U. Baranger, and G. Finkelstein, Nat. Phys. **16**, 862 (2020).
[42] A. Altland, Y. Gefen, and B. Rosenow, Phys. Rev. B **92**, 085124 (2015).
[43] M. A. Cazalilla, F. Sols, and F. Guinea, Phys. Rev. Lett. **97**, 076401 (2006).
[44] A. J. Friedman, arXiv:1910.06371.
[45] Z. Ristivojevic and T. Nattermann, Phys. Rev. Lett. **101**, 016405 (2008).
[46] A. V. Shytov, L. S. Levitov, and B. I. Halperin, Phys. Rev. Lett. **80**, 141 (1998).
[47] A. M. Chang, L. N. Pfeiffer, and K. W. West, Phys. Rev. Lett. **77**, 2538 (1996).
[48] M. Grayson, D. C. Tsui, L. N. Pfeiffer, K. W. West, and A. M. Chang, Phys. Rev. Lett. **80**, 1062 (1998).
[49] M. Grayson, D. C. Tsui, L. N. Pfeiffer, K. W. West, and A. M. Chang, Phys. Rev. Lett. **86**, 2645 (2001).
[50] T. Giamarchi, *Quantum Physics in One Dimension*, International Series of Monographs on Physics (Oxford University Press, Oxford, UK, 2003).
[51] X. Wen, *Quantum Field Theory of Many-Body Systems: From the Origin of Sound to an Origin of Light and Electrons*, Oxford Graduate Texts (Oxford University Press, Oxford, U.K., 2004).
[52] See Supplemental Material at http://link.aps.org/supplemental/10.1103/PhysRevB.107.L161105 for complete derivations and technical points of discussion.
[53] K. I. Bolotin, F. Ghahari, M. D. Shulman, H. L. Stormer, and P. Kim, Nature (London) **462**, 196 (2009).
[54] Y. Oreg and A. M. Finkel'stein, Phys. Rev. Lett. **74**, 3668 (1995).
[55] C. L. Kane, M. P. A. Fisher, and J. Polchinski, Phys. Rev. Lett. **72**, 4129 (1994).